Acta Cryst E CRYSTALLOGRAPHIC COMMUNICATIONS

ISSN 2056-9890

Crystal structure, Hirshfeld surface analysis, DFT and molecular docking studies of 4′-(benzyloxy)-[1,1′-biphenyl]-3-carboxylic acid

M. Harish Kumar,[a] M. Vinduvahini,[b] H. T. Srinivasa,[c] H. C. Devarajegowda[a] and B. S. Palakshamurthy[d]*

[a]Department of Physics, Yuvaraja's College, University of Mysore, Mysore, 570005, Karnataka, India, [b]Department of Physics, Maharani's Science College for Women (Autonomous) Mysore, Karnataka, 570005, India, [c]Raman Research Institute, C. V. Raman Avenue, Sadashivanagar, Bangalore, Karnataka, India, and [d]Department of PG Studies and Research in Physics, Albert Einstein Block, UCS, Tumkur University, Tumkur, Karnataka, 572103, India. *Correspondence e-mail: palaksha.bspm@gmail.com

Received 14 January 2025
Accepted 5 February 2025

Edited by X. Hao, Institute of Chemistry, Chinese Academy of Sciences

Keywords: crystal structure; Hirshfeld surface; DFT studies; molecular docking; benzyloxy; biphenyl carboxylic acid.

CCDC reference: 2421495

Supporting information: this article has supporting information at journals.iucr.org/e

In the title compound, $C_{20}H_{16}O_3$, intramolecular C— H···O hydrogen bonds are observed. The dihedral angles between the aromatic benzoic acid ring and the two adjacent aromatic rings are 26.09 (4) and 69.93 (8)°, while the dihedral angle between the aromatic rings connected by the C—O—C—C [torsion angle = −175.9 (2)°] link is 89.11 (3)°. In the crystal, inversion dimers linked by pairs of O—H···O hydrogen bonds generate $R_2^2(8)$ ring motifs. These dimers are further linked by C—H···π interactions, forming molecular sheets along (010). The molecular structure was optimized by density functional theory (DFT) at the B3LYP/6–311+ G(d,p) level and the bond lengths, angles and torsion angles were compared with experimental values obtained by X-ray diffraction. The HOMO and LUMO were calculated, the energy gap between them being 4.3337 eV. Further, the intermolecular interactions were quantified using Hirshfeld surface analysis and fingerprint plots and energy frameworks were generated. The two-dimensional fingerprint plots indicate that the major contributions to the crystal packing are from H···H (39.7%), H···C (39.0%) and H···O (18.0%) interactions. The energy framework calculations reveal that the dispersion energy (E_{dis}= 201.0 kJ mol^{-1}) dominates the other energies. Molecular docking studies were carried out for the title compound as a ligand and the SARS-Covid-2 (PDB ID:8BEC) protein, specifically the Omicron variant, was used as a receptor giving a binding affinity of −7.6 kcal mol^{-1}.

1. Chemical context

The biphenyl moiety forms an important intermediary of compounds having profound pharmacological activities (Jain *et al.*, 2017). Biphenyl-derived drugs are found to exhibit anti-cancer, anti-diabetic, anti-inflammatory and various therapeutic activities, and represent a well-known rigid core moiety in pharmacological applications. Biphenyl carboxylic acid derivatives have been described as a new class of anti-resorptive drugs with potential therapeutic benefits for preventing and treating diseases associated with osteoclast activation such as osteoporosis, cancer-induced bone disease and Paget's disease (Idris *et al.*, 2009; van't Hof *et al.*, 2004) and exhibit anti-hypertensive activity (Sharma *et al.*, 2010). Biphenyl-2-carboxylic acid and biphenyl-4-carboxylic acids exhibit different levels of activity in cell toxicity tests and inhibit the tubulin polymerization process (Mukherjee *et al.*, 2016; Mahale *et al.*, 2014). Hydrazide-hydrazone-containing biphenyl compounds demonstrate potential anti-microbial activity (Deep *et al.*, 2010). Biphenyl imidazole derivatives exhibit excellent antifungal activity (Zhao *et al.*, 2017) while

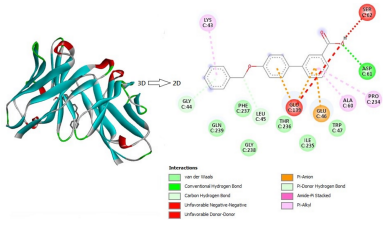

benzyloxy triazole derivatives display moderate-to-excellent antibacterial activity (Kaushik *et al.*, 2018), The organic nitrate-containing benzyloxy isonipecotanilide derivatives exhibit strong NO-mediated vasodilatory effects on pre-contracted rat aorta strips (de Candia *et al.*, 2015), and studies on bezyloxy oxopyridin benzoate derivatives have revealed that further investigations on these compounds could lead to new compounds that may be considered as anti-malarial or cytotoxic agents (Mohebi *et al.*, 2022). As part of our studies in this area, our team is working to explore crystal structures of interest for biological studies.

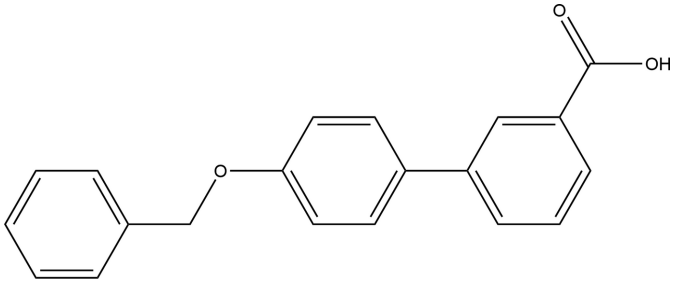

2. Structural commentary

The structure of the title compound is shown in Fig. 1. The dihedral angle between the aromatic ring of the benzyloxy group (C1–C7) and the (C8–C13) ring in the biphenyl carboxylic acid group is 89.11 (2)°, while the angle between the benzyloxy group (C1–C7) and the (C14–C19) ring in the biphenyl carboxylic acid group is 69.93 (8)°. The dihedral angle between the adjacent rings within the biphenyl carboxylic acid group (C8–C13 and C14–C19) is 26.09 (4)°. The torsion angle within the benzyloxy moiety (C1—C7—O1—C8) is −175.9 (2)°. Otherwise, the bond distances and angles may be regarded as normal. Intramolecular C—H···O hydrogen bonds occur.

3. Supramolecular features

In the crystal, weak O3—H3*A*···O2 hydrogen bonding leads to the formation of inversion dimers, which are linked by pairs of O—H···O hydrogen bonds generating an $R_2^2(8)$ ring motif (Fig. 2, Table 1). The O3—H3*A* distance of 1.20 (5) Å is quite a large as a result of tensile stress between the dimers. The tensile force between the two dimers can increase the donor–hydrogen distance, obviously weakening the hydrogen bond. In addition, the packing is consolidated by four C—H···π interactions (Table 1, Fig. 3).

Table 1
Hydrogen-bond geometry (Å, °).

*Cg*1 and *Cg*2 are the centroids of the C1–C6 and C8–C12 rings, respectively,

D—H···*A*	*D*—H	H···*A*	*D*···*A*	*D*—H···*A*
C15—H15···O2	0.93	2.48	2.791 (3)	100
C17—H17···O3	0.93	2.48	2.767 (4)	98
O3—H3*A*···O2^{i}	1.20 (5)	1.42 (5)	2.617 (3)	175 (4)
C3—H3···*Cg*1^{ii}	0.93	2.88	3.711 (4)	149
C6—H6···*Cg*1^{iii}	0.93	2.77	3.588 (4)	147
C9—H9···*Cg*2^{iv}	0.93	2.86	3.667 (3)	146
C12—H12···*Cg*2^{v}	0.93	2.81	3.629 (3)	147

Symmetry codes: (i) $-x+1, y, -z+\frac{1}{2}$; (ii) $x, -y, z-\frac{1}{2}$; (iii) $x, -y+1, z-\frac{3}{2}$; (iv) $x, -y+1, z-\frac{1}{2}$; (v) $x, -y, z-\frac{3}{2}$.

4. Database survey

A search of the Cambridge Structural Database (CSD version 2.0.4, December 2019; Groom *et al.*, 2016) for molecules containing [1,1′-biphenyl]-3-carboxylic acid resulted in eleven matches. Of these, five compounds, CUFYEL (Guo *et al.*, 2024), HUJZIY, HUJZOE and HUJZUK (O'Malley *et al.*, 2020) and SEBMOF (Barbas *et al.*, 2022) have dihedral angles between the aromatic rings of the biphenyl carboxylic acid group ranging from 40.99 (2) to 44.58 (3)°. In three compounds, ILURAL (Hurlock *et al.*, 2021), QAKHOD (O'Malley *et al.*, 2021 and RADDIN (Doiron *et al.*, 2020), one

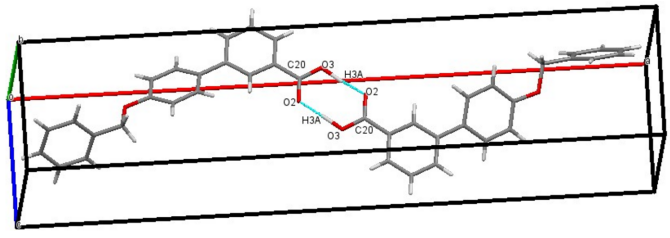

Figure 2
Molecular packing of the title compound, showing the O—H···O hydrogen bonds that generate inversion dimers with $R_2^2(8)$ ring motifs.

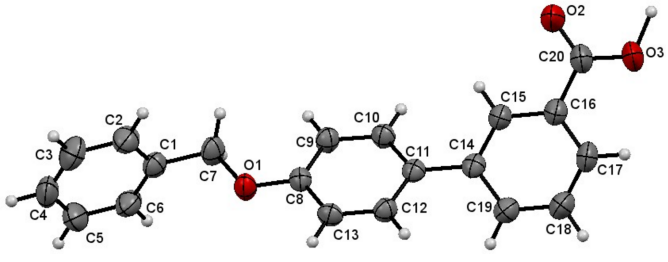

Figure 1
Molecular structure of the title compound, showing the atom-labeling scheme. Displacement ellipsoids are drawn at the 50% probability level.

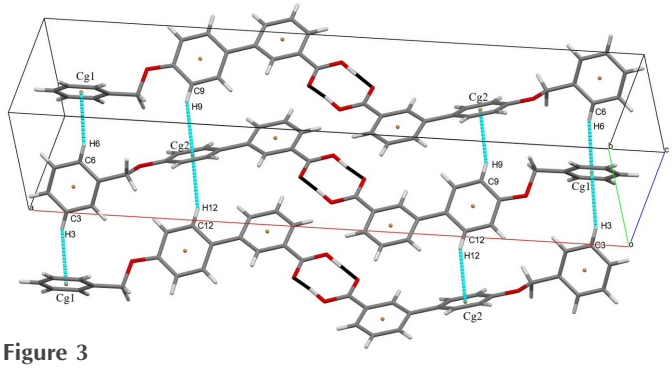

Figure 3
Packing of the molecules showing C—H···π interactions.

of the dihedral angles lies between 54.71 (3) and 59.70 (6)°. In the title compound, this dihedral angle is 26.09 (4)°. The relatively small dihedral angle may be attributed to the presence of the bulky benzyloxy group attached to the biphenyl carboxylic acid group and may also be a result of the tensile force between the two dimers. For molecules containing the benzyloxy fragment, a search resulted in thirty matches: in all of these, the torsion angle of the linking C—O—C—C unit indicates a conformation close to *anti*.

5. Synthesis and crystallization

Methyl 4′-(benzyloxy)-[1,1′-biphenyl]-3-carboxylate was added in a round-bottom flask containing a solution (5%, 1.25 g of KOH in 25 mL of ethanol) of potassium hydroxide in water and a small excess amount of ethyl alcohol. The whole reaction mixture was refluxed at 373 K for 6 h, cooled and poured into ice-cold hydrochloric acid. The product 4′-(benzyloxy)-[1,1′-biphenyl]-3-carboxylic acid separated out as a solid, which was filtered and then washed with water to remove excess hydrochloric acid. Finally, single crystals suitable for X-ray diffraction studies were grown in pure ethanol at room temperature. For the detailed synthesis procedure, see Radhika *et al.* (2011). ^{1}H NMR: ($CDCl_3$, δ): 12 (*s*, 1H, –COOH), 8.74-8.24 (*m*, 2H, Ar-H), 7.85–7.78 (*m*, 4H, Ar-H), 7.48–7.02 (*m*, 7H, Ar-H), 5.0 (*s*, 2H, –OCH_2–) ppm.

6. Hirshfeld surface analysis

Hirshfeld surface analysis (Hirshfeld, 1977; Spackman & Jayatilaka, 2009) was performed to visualize and quantify the intermolecular interactions in the title molecule using *CrystalExplorer* (Spackman *et al.*, 2021). The Hirshfeld surface mapped over d_{norm} is shown in Fig. 4 with colors representing intermolecular interactions on the surface. The red regions are attributed to the O2—H2···O3 interaction. The two-dimensional fingerprint plots indicate that the major contributions to the crystal packing are from H···H (39.7%), C···H/H···C (39%) and O···H/H···O (18%) as shown in Fig. 5. The net interaction energies were calculated as E_{ele} = 145.6 kJ mol^{-1}, E_{pol} = 47.3 kJ mol^{-1}, E_{dis} = 201.0 kJ mol^{-1}, E_{rep} = 83.6 kJ mol^{-1} and total interaction energy E_{tot} = 308.0 kJ mol^{-1}. The topology of the energy frameworks for the Coulombic, dispersion and total energies are shown in Fig. 6. Higher dispersion energy can affect the reactivity of the molecules, particularly in biological processes such as docking the ligand with a protein. The dispersion energy influences the binding affinity of the ligand by providing an additional attractive force.

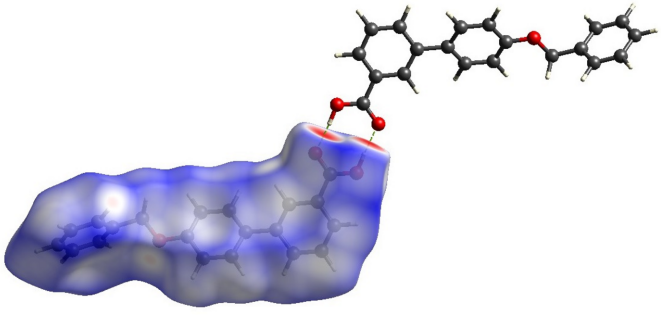

Figure 4
The Hirshfeld surface of the title compound with the dashed lines indicating the O—H···O hydrogen bonds that form inversion dimers.

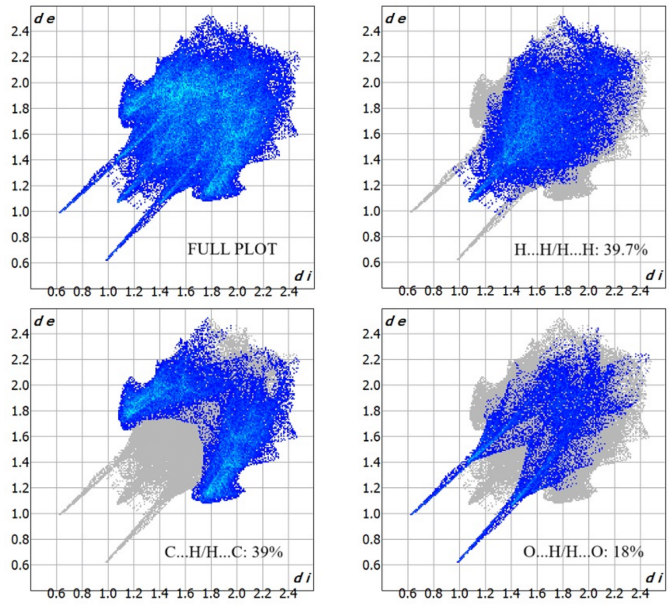

Figure 5
The two-dimensional fingerprint plots of the title molecule showing all interactions and those delineated into H···H, C···H/H···C and H···O/O···H.

7. DFT Studies

The HOMO–LUMO levels are valuable for understanding the molecule's interactions in chemical reactions, electronic transitions, and stability. The molecule was constructed using

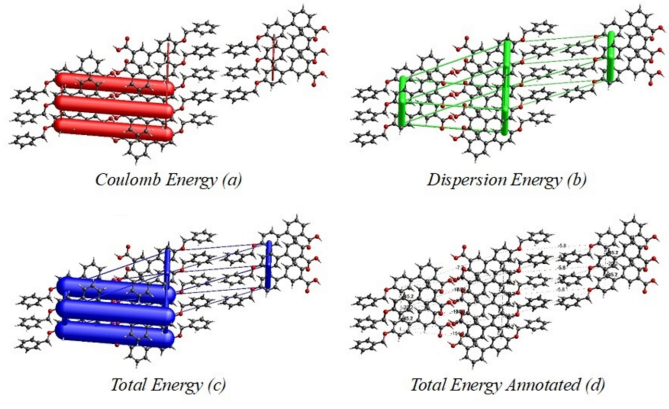

Figure 6
The energy frameworks for interaction energies in the title compound, (*a*) Coulombic energy, (*b*) dispersion energy, (*c*) total energy and (*d*) total energy annotated.

Table 2
Selected bond lengths, angles and torsion angles (Å, °).

Parameter	SCXRD	DFT
O1—C8	1.366 (3)	1.36392
O1—C7	1.437 (3)	1.43631
O2—C20	1.241 (3)	1.20944
O3—C20	1.270 (3)	1.35882
C8—O1—C7	117.75 (19)	118.64625
O1—C8—C13	115.7 (2)	115.79634
O1—C8—C9	125.3 (2)	124.91696
C13—C8—C9	119.0 (2)	119.28680
C7—O1—C8—C13	179.0 (2)	179.2209
C7—O1—C8—C9	−0.5 (4)	−0.79351
C8—O1—C7—C1	−175.9 (2)	−178.9820
O1—C8—C13—C12	−178.5 (2)	−179.9223

Table 3
The energy values (eV) of global reactivity descriptors for the title compound.

*E*_HOMO_	−6.0801
*E*_LUMO_	−1.7464
Energy gap (eV)	4.3337
Ionization Energy (*I*)	6.0801
Electron affinity (*A*)	1.7464
Electronegativity (χ)	3.91325
Chemical hardness (η)	2.16685
Chemical softness (*S*)	0.231 eV^{-1}
Chemical potential (μ)	−3.91325
Electrophilicity index (ω)	3.534

Gaussview 06 and optimized with the B3LYP/6-311++G(d,p) model in *Gaussian 09* (Frisch *et al.*, 2009). The optimized structure is illustrated in Fig. 7. The optimized bond lengths, angles and torsion angles were compared with those obtained from SCXRD data (Table 2) and are found to be in good agreement with each other. The tensile force between the two dimers is not taken into the account in the quantum calculations, so there is a common donor–hydrogen distance around the carboxylic group in the DFT calculations. Fig. 8 shows the HOMO and LUMO and their energy gap in the title compound. In the HOMO, electron density is mainly concentrated on the biphenyl rings, with a smaller presence on the oxygen atom in the benzyloxy group. In the LUMO, the electron density is primarily located on the benzoic acid portion of the biphenyl group. The HOMO and LUMO

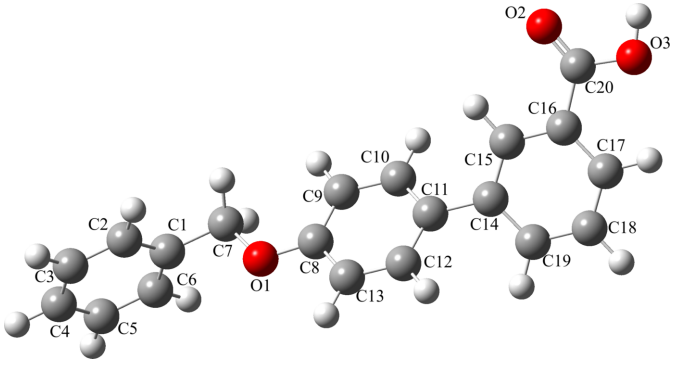

Figure 7
The optimized structure of the title compound generated using *Gaussian 09* at the B3LYP/6–311++G(d,p) level.

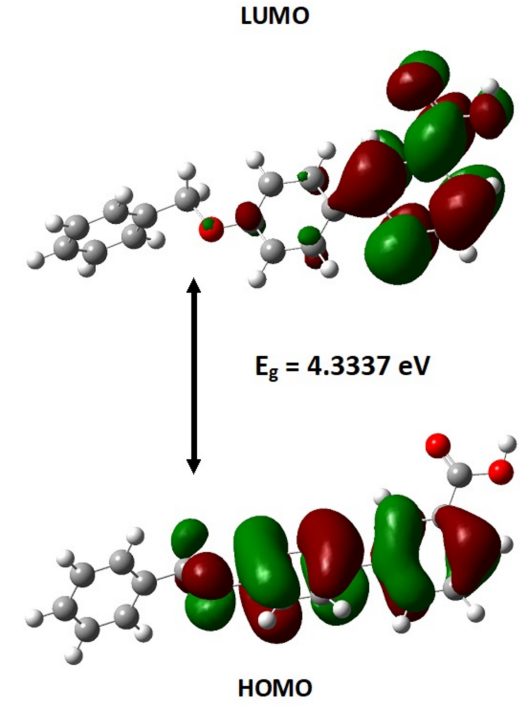

Figure 8
The HOMO and LUMO molecular orbitals of the title compound.

energies are −6.0814 eV and −1.7466 eV, respectively, resulting in an energy gap (ΔE) of 4.3347 eV. Reactivity descriptors including ionization energy (I), electron affinity (A), electronegativity (χ), chemical hardness (η), chemical potential (μ), electrophilicity index (ω), and chemical softness (S) are presented in Table 3. The electrophilicity index value of 3.534 eV indicates that the molecule exhibits strong electrophilicity.

8. Molecular electrostatic potential

The molecular electrostatic potential surface (MEPS) helps to visualize the electrostatic environment around a molecule and is illustrated for the title compound in Fig. 9. The electron-rich

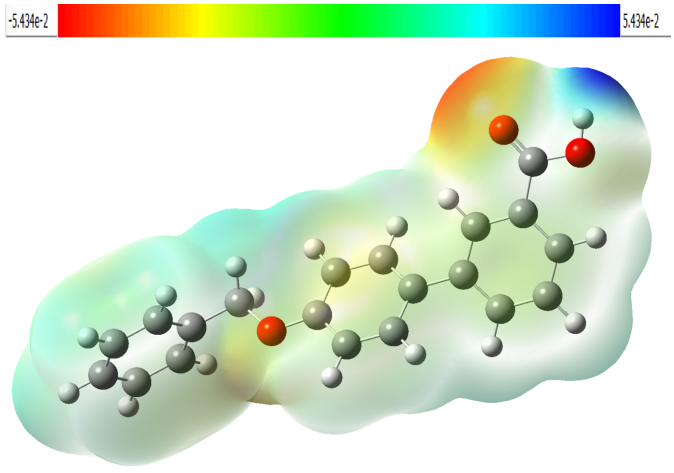

Figure 9
The molecular electrostatic potential surface of the title compound.

part with a partial negative charge is shown by the combination of red and pale-yellow regions on the MEPS over the oxygen atom of the carboxylic acid moiety and is an active site for electrophilic attack, which is essential for biological recognition and hydrogen-bonding interactions. The bright-blue region on the MEPS over the hydrogen atom of the carboxylic acid moiety is an active site for possible nucleophilic attack (Friesner *et al.*, 2006).

9. Molecular docking studies

The docking of a receptor protein, specifically the Omicron variant (PDB ID:8BEC, SARS-COV2-VARIANT), with the synthesized ligand shows a very good binding affinity of −7.6 kcal mol^{-1}. *AutoDock Vina* (Morris *et al.*, 2009) was used for theoretical calculations and the interaction was generated by *Discovery Studio Visualizer* (Biovia, 2017). A 2D view of the docking interactions shows one conventional bond with ACP C:61 and two π-donor hydrogen bonds with GLY C:44 and LEU C:45. The higher dispersion energy influences the ligand to have conformational stability with the protein. The idea of docking of the protein molecules with the centroids of the ligands can be used in structure-based drug design. Modifications in the synthesized ligands by varying functional groups and atoms can easily achieve a very good binding affinity with the target protein. In the title ligand we can see three centroids, of which *Cg*1 and *Cg*2 (the centroids of the C1–C6 and C8–C12 rings) play significant role in the intermolecular interactions. Meanwhile these act as anchor points for the ligand, the interaction with these centroids and GLU C:139, GLU C:46 and ALU C:60 PRO C:234 amino acids forming π–anion and π–donor hydrogen bonds, respectively. In addition to these interactions, a few van der Waals interactions can be seen around the ligand and unfavorable interactions are observed at the –OH group; these are shown in Fig. 10.

Table 4
Experimental details.

Crystal data	
Chemical formula	$C_{20}H_{16}O_3$
M_r	304.33
Crystal system, space group	Monoclinic, *P*2/*c*
Temperature (K)	299
a, *b*, *c* (Å)	31.9237 (13), 7.0199 (3), 6.9184 (3)
β (°)	91.864 (1)
V (Å^3)	1549.60 (11)
Z	4
Radiation type	Mo $K\alpha$
μ (mm^{-1})	0.09
Crystal size (mm)	0.31 × 0.27 × 0.18
Data collection	
Diffractometer	Bruker *SMART* APEXII CCD
Absorption correction	Multi-scan (*SADABS*; Krause *et al.*, 2015)
T_{min}, T_{max}	0.972, 0.983
No. of measured, independent and observed [$I > 2\sigma(I)$] reflections	35610, 2760, 2207
R_{int}	0.072
(sin $\theta/\lambda)_{max}$ (Å^{-1})	0.597
Refinement	
$R[F^2 > 2\sigma(F^2)]$, $wR(F^2)$, S	0.069, 0.162, 1.13
No. of reflections	2760
No. of parameters	212
H-atom treatment	H atoms treated by a mixture of independent and constrained refinement
$\Delta\rho_{max}$, $\Delta\rho_{min}$ (e Å^{-3})	0.18, −0.20

Computer programs: *APEX2* and *SAINT* (Bruker, 2017), *SHELXT2018* (Sheldrick, 2015*a*), *SHELXL2019/2* (Sheldrick, 2015*b*) and *Mercury* (Macrae *et al.*, 2020).

10. Refinement

Crystal data, data collection and structure refinement details are summarized in Table 4. The hydrogen atom of the hydroxyl group was freely refined. All other H atoms were positioned with idealized geometry and refined using a riding model with C—H = 0.93–0.97 Å and U_{iso}(H) = 1.2U_{eq}(C) or 1.5U_{eq}(methyl C).

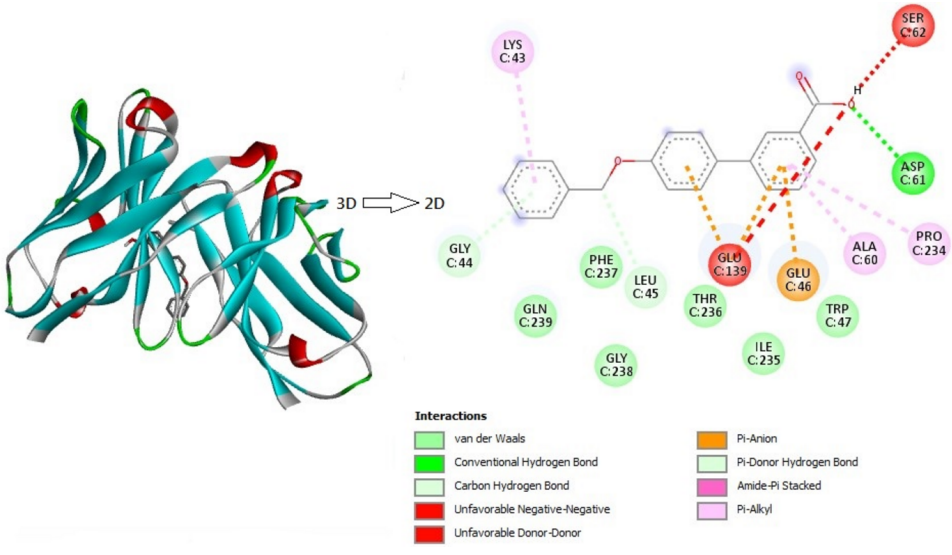

Figure 10
The three-dimensional and two-dimensional views of various interactions between the title molecule (ligand) and the receptor protein SARS-Covid-2 (PDB ID:8BEC).

Acknowledgements

The authors extend their gratitude to Kishore and Shashikanth, SSCU, IISc for their help in collecting SCXRD data.

Funding information

Funding for this research was provided by: Vission Group of Science and Technology (award No. GRD319 to B. S. Palakshamurthy).

References

Barbas, R., Font-Bardia, M., Ballesteros, A., Arsequell, G., Prohens, R. & Frontera, A. (2022). *CrystEngComm*, **24**, 3057–3063.
Biovia (2017). *Discovery Studio Visualizer*. Biovia, San Diego, CA, USA.
Bruker (2017). *APEX2* and *SAINT*. Bruker AXS Inc., Madison, Wisconsin, USA.
Candia, M. de, Marini, E., Zaetta, G., Cellamare, S., Di Stilo, A. & Altomare, C. D. (2015). *Eur. J. Pharm. Sci.* **72**, 69–80.
Deep, A., Jain, S., Sharma, P. C., Verma, P., Kumar, M. & Dora, C. P. (2010). *Synthesis*, **182**, 183.
Doiron, J. E., Le, C. A., Bacsa, J., Breton, G. W., Martin, K. L., Aller, S. G. & Turlington, M. (2020). *ChemMedChem*, **15**, 1720–1730.
Friesner, R. A., Murphy, R. B., Repasky, M. P., Frye, L. L., Greenwood, J. R., Halgren, T. A., Sanschagrin, P. C. & Mainz, D. T. (2006). *J. Med. Chem.* **49**, 6177–6196.
Frisch, M. J., Trucks, G. W., Schlegel, H. B., Scuseria, G. E., Robb, M. A., Cheeseman, J. R., Scalmani, G., Barone, V., Mennucci, B., Petersson, G. A., Nakatsuji, H., Caricato, M., Li, X., Hratchian, H. P., Izmaylov, A. F., Bloino, J., Zheng, G., Sonnenberg, J. L., Hada, M., Ehara, M., Toyota, K., Fukuda, R., Hasegawa, J., Ishida, M., Nakajima, T., Honda, Y., Kitao, O., Nakai, H., Vreven, T., Montgomery, J. A. Jr, Peralta, J. E., Ogliaro, F., Bearpark, M., Heyd, J. J., Brothers, E., Kudin, K. N., Staroverov, V. N., Kobayashi, R., Normand, J., Raghavachari, K., Rendell, A., Burant, J. C., Iyengar, S. S., Tomasi, J., Cossi, M., Rega, N., Millam, J. M., Klene, M., Knox, J. E., Cross, J. B., Bakken, V., Adamo, C., Jaramillo, J., Gomperts, R., Stratmann, R. E., Yazyev, O., Austin, A. J., Cammi, R., Pomelli, C., Ochterski, J. W., Martin, R. L., Morokuma, K., Zakrzewski, V. G., Voth, G. A., Salvador, P., Dannenberg, J. J., Dapprich, S., Daniels, A. D., Farkas, Ö., Foresman, J. B., Ortiz, J. V., Cioslowski, J. & Fox, D. J. (2009). *Gaussian 09*. Gaussian Inc., Wallingford CT, USA.
Groom, C. R., Bruno, I. J., Lightfoot, M. P. & Ward, S. C. (2016). *Acta Cryst.* B**72**, 171–179.
Guo, X., Li, T., Cao, X. & Zhang, W. (2024). *Z. Krist. New Cryst. Struct*. **239**, 957–959.
Hirshfeld, H. L. (1977). *Theor. Chim. Acta*, **44**, 129–138.
Hurlock, M. J., Lare, M. F. & Zhang, Q. (2021). *Inorg. Chem.* **60**, 2503–2513.
Idris, A. I., Greig, I. R., Bassonga-Landao, E., Ralston, S. H. & van 't Hof, R. J. (2009). *Endocrinology*, **150**, 5–13.
Jain, Z. J., Gide, P. S. & Kankate, R. S. (2017). *Arab. J. Chem.* **10**, S2051–S2066.
Kaushik, C. P., Pahwa, A., Kumar, D., Kumar, A., Singh, D., Kumar, K. & Luxmi, R. (2018). *J. Heterocycl. Chem.* **55**, 1720–1728.
Krause, L., Herbst-Irmer, R., Sheldrick, G. M. & Stalke, D. (2015). *J. Appl. Cryst.* **48**, 3–10.
Macrae, C. F., Sovago, I., Cottrell, S. J., Galek, P. T. A., McCabe, P., Pidcock, E., Platings, M., Shields, G. P., Stevens, J. S., Towler, M. & Wood, P. A. (2020). *J. Appl. Cryst.* **53**, 226–235.
Mahale, S., Bharate, S. B., Manda, S., Joshi, P., Bharate, S. S., Jenkins, P. R., Vishwakarma, R. A. & Chaudhuri, B. (2014). *J. Med. Chem.* **57**, 9658–9672.
Mohebi, M., Fayazi, N., Esmaeili, S., Rostami, M., Bagheri, F., Aliabadi, A., Asadi, P. & Saghaie, L. (2022). *Res. Pharm. Sci*. **17**, 252–264.
Morris, G. M., Huey, R., Lindstrom, W., Sanner, M. F., Belew, R. K., Goodsell, D. S. & Olson, A. J. (2009). *J. Comput. Chem.* **30**, 27852791.
Mukherjee, S., Chatterjee, S., Poddar, A., Bhattacharyya, B. & Gupta, S. (2016). *J. Taibah Univ. Sci.* **10**, 839–849.
O'Malley, C., Erxleben, A., Kellehan, S. & McArdle, P. (2020). *Chem. Commun.* **56**, 5657–5660.
O'Malley, C., Erxleben, A., McArdle, P. & Simmie, J. M. (2021). *Cryst. Growth Des.* **21**, 23–27.
Radhika, S., Srinivasa, H. T. & Sadashiva, B. K. (2011). *Liq. Cryst.* **38**, 785–792.
Sharma, M. C., Kohli, D. V. & Sharma, S. (2010). *Digest J. Nanomaterials Biostructures*, **5**, 605–621.
Sheldrick, G. M. (2015*a*). *Acta Cryst.* A**71**, 3–8.
Sheldrick, G. M. (2015*b*). *Acta Cryst.* C**71**, 3–8.
Spackman, M. A. & Jayatilaka, D. (2009). *CrystEngComm*, **11**, 19–32.
Spackman, P. R., Turner, M. J., McKinnon, J. J., Wolff, S. K., Grimwood, D. J., Jayatilaka, D. & Spackman, M. A. (2021). *J. Appl. Cryst.* **54**, 1006–1011.
van't Hof, R. J., Idris, A. I., Ridge, S. A., Dunford, J., Greig, I. R. & Ralston, S. H. (2004). *J. Bone Miner. Res.* **19**, 1651–1660.
Zhao, D., Zhao, S., Zhao, L., Zhang, X., Wei, P., Liu, C., Hao, C., Sun, B., Su, X. & Cheng, M. (2017). *Bioorg. Med. Chem.* **25**, 750–758.

supporting information

Acta Cryst. (2025). E**81** [https://doi.org/10.1107/S2056989025001021]

Crystal structure, Hirshfeld surface analysis, DFT and molecular docking studies of 4′-(benzyloxy)-[1,1′-biphenyl]-3-carboxylic acid

M. Harish Kumar, M. Vinduvahini, H. T. Srinivasa, H. C. Devarajegowda and B. S. Palakshamurthy

Computing details

3-[4-(Benzyloxy)phenyl]benzoic acid

Crystal data

$C_{20}H_{16}O_3$
M_r = 304.33
Monoclinic, $P2/c$
Hall symbol: -P 2yc
a = 31.9237 (13) Å
b = 7.0199 (3) Å
c = 6.9184 (3) Å
β = 91.864 (1)°
V = 1549.60 (11) Å^3
Z = 4
$F(000)$ = 640
D_x = 1.304 Mg m^{-3}
Mo $K\alpha$ radiation, λ = 0.71073 Å
Cell parameters from 2207 reflections
θ = 2.0–25.0°
μ = 0.09 mm^{-1}
T = 299 K
Prism, colourless
0.31 × 0.27 × 0.18 mm

Data collection

Bruker SMART APEXII CCD diffractometer
Radiation source: fine-focus sealed tube
Graphite monochromator
Detector resolution: 1.09 pixels mm^{-1}
φ and Ω scans
Absorption correction: multi-scan (SADABS; Krause *et al.*, 2015)
T_{min} = 0.972, T_{max} = 0.983
35610 measured reflections
2760 independent reflections
2207 reflections with $I > 2\sigma(I)$
R_{int} = 0.072
θ_{max} = 25.1°, θ_{min} = 2.6°
h = −38→38
k = −8→8
l = −8→8

Refinement

Refinement on F^2
Least-squares matrix: full
$R[F^2 > 2\sigma(F^2)]$ = 0.069
$wR(F^2)$ = 0.162
S = 1.13
2760 reflections
212 parameters
0 restraints
0.12 constraints
Primary atom site location: structure-invariant direct methods
Secondary atom site location: difference Fourier map
Hydrogen site location: mixed
H atoms treated by a mixture of independent and constrained refinement
$w = 1/[\sigma^2(F_o^2) + (0.0584P)^2 + 1.0677P]$ where $P = (F_o^2 + 2F_c^2)/3$
$(\Delta/\sigma)_{max} < 0.001$
$\Delta\rho_{max}$ = 0.18 e Å^{-3}
$\Delta\rho_{min}$ = −0.20 e Å^{-3}

Special details

Geometry. All esds (except the esd in the dihedral angle between two l.s. planes) are estimated using the full covariance matrix. The cell esds are taken into account individually in the estimation of esds in distances, angles and torsion angles; correlations between esds in cell parameters are only used when they are defined by crystal symmetry. An approximate (isotropic) treatment of cell esds is used for estimating esds involving l.s. planes.

Fractional atomic coordinates and isotropic or equivalent isotropic displacement parameters (Å²)

	x	*y*	*z*	U_{iso}*/U_{eq}
O1	0.82388 (5)	0.2450 (3)	0.2817 (2)	0.0451 (5)
O2	0.55270 (6)	0.2739 (4)	0.2404 (3)	0.0803 (8)
O3	0.51314 (6)	0.2653 (5)	0.4950 (3)	0.0951 (10)
C8	0.78393 (7)	0.2524 (3)	0.3464 (3)	0.0348 (6)
C12	0.73839 (7)	0.1552 (4)	0.5975 (3)	0.0383 (6)
H12	0.734753	0.091923	0.713867	0.046*
C13	0.77746 (8)	0.1606 (4)	0.5216 (4)	0.0388 (6)
H13	0.799867	0.102365	0.587397	0.047*
C14	0.66164 (7)	0.2393 (3)	0.5886 (3)	0.0365 (6)
C10	0.71123 (8)	0.3348 (4)	0.3318 (4)	0.0388 (6)
H10	0.688949	0.394984	0.266940	0.047*
C11	0.70391 (7)	0.2422 (3)	0.5053 (3)	0.0348 (6)
C9	0.75043 (7)	0.3408 (4)	0.2519 (4)	0.0391 (6)
H9	0.754192	0.403897	0.135543	0.047*
C15	0.62556 (8)	0.2555 (4)	0.4737 (4)	0.0431 (6)
H15	0.628038	0.268632	0.340789	0.052*
C16	0.58606 (8)	0.2530 (4)	0.5484 (4)	0.0451 (7)
C1	0.87677 (8)	0.2945 (4)	0.0553 (4)	0.0417 (6)
C6	0.90842 (9)	0.4146 (4)	0.1193 (4)	0.0522 (7)
H6	0.901833	0.522717	0.189822	0.063*
C19	0.65636 (9)	0.2203 (4)	0.7877 (4)	0.0468 (7)
H19	0.679840	0.208984	0.870101	0.056*
C7	0.83194 (8)	0.3350 (4)	0.1001 (4)	0.0487 (7)
H7A	0.827368	0.471270	0.108922	0.058*
H7B	0.813364	0.284253	−0.001031	0.058*
C17	0.58190 (9)	0.2345 (4)	0.7471 (4)	0.0540 (8)
H17	0.555481	0.233411	0.799881	0.065*
C20	0.54871 (9)	0.2661 (5)	0.4180 (4)	0.0566 (8)
C2	0.88725 (9)	0.1367 (4)	−0.0504 (4)	0.0528 (7)
H2	0.866309	0.054912	−0.096613	0.063*
C18	0.61711 (9)	0.2180 (5)	0.8637 (4)	0.0566 (8)
H18	0.614462	0.205111	0.996566	0.068*
C5	0.94942 (9)	0.3774 (5)	0.0806 (4)	0.0626 (9)
H5	0.970380	0.459793	0.125360	0.075*
C3	0.92875 (10)	0.0985 (5)	−0.0889 (5)	0.0626 (9)
H3	0.935578	−0.009465	−0.159101	0.075*
C4	0.95967 (9)	0.2195 (5)	−0.0237 (4)	0.0617 (9)
H4	0.987522	0.194607	−0.050102	0.074*
H3A	0.4838 (16)	0.265 (7)	0.382 (7)	0.155 (19)*

Atomic displacement parameters (Å²)

	U^{11}	U^{22}	U^{33}	U^{12}	U^{13}	U^{23}
O1	0.0345 (10)	0.0588 (12)	0.0423 (10)	0.0053 (8)	0.0067 (7)	0.0124 (9)
O2	0.0398 (12)	0.157 (3)	0.0447 (13)	−0.0007 (13)	0.0056 (9)	0.0059 (14)
O3	0.0307 (11)	0.199 (3)	0.0562 (14)	0.0012 (15)	0.0094 (10)	−0.0046 (17)
C8	0.0322 (12)	0.0346 (13)	0.0379 (13)	−0.0004 (10)	0.0043 (10)	−0.0009 (11)
C12	0.0399 (14)	0.0415 (14)	0.0336 (13)	0.0013 (11)	0.0038 (10)	0.0057 (11)
C13	0.0373 (14)	0.0416 (14)	0.0372 (14)	0.0057 (11)	−0.0036 (11)	0.0057 (11)
C14	0.0389 (14)	0.0332 (13)	0.0378 (13)	−0.0023 (11)	0.0049 (11)	−0.0026 (11)
C10	0.0352 (13)	0.0431 (15)	0.0381 (14)	0.0049 (11)	0.0009 (10)	0.0062 (12)
C11	0.0365 (13)	0.0327 (13)	0.0353 (13)	−0.0019 (11)	0.0025 (10)	−0.0020 (11)
C9	0.0384 (14)	0.0410 (14)	0.0383 (14)	0.0035 (11)	0.0045 (11)	0.0079 (12)
C15	0.0371 (14)	0.0558 (17)	0.0366 (14)	−0.0009 (12)	0.0059 (11)	−0.0024 (13)
C16	0.0390 (14)	0.0552 (17)	0.0414 (15)	−0.0005 (12)	0.0077 (11)	−0.0035 (13)
C1	0.0416 (14)	0.0467 (15)	0.0371 (14)	−0.0021 (12)	0.0068 (11)	0.0070 (12)
C6	0.0550 (17)	0.0605 (18)	0.0415 (15)	−0.0071 (14)	0.0090 (13)	−0.0110 (14)
C19	0.0480 (16)	0.0544 (17)	0.0381 (15)	−0.0021 (13)	0.0032 (12)	−0.0010 (13)
C7	0.0443 (15)	0.0581 (17)	0.0442 (16)	0.0034 (13)	0.0101 (12)	0.0178 (14)
C17	0.0401 (15)	0.074 (2)	0.0490 (17)	−0.0001 (14)	0.0167 (13)	−0.0016 (15)
C20	0.0344 (15)	0.085 (2)	0.0509 (18)	0.0000 (15)	0.0084 (12)	−0.0004 (16)
C2	0.0525 (17)	0.0566 (18)	0.0496 (17)	−0.0112 (14)	0.0054 (13)	−0.0063 (14)
C18	0.0515 (18)	0.081 (2)	0.0379 (15)	−0.0022 (15)	0.0094 (13)	−0.0013 (15)
C5	0.0447 (17)	0.087 (2)	0.0561 (19)	−0.0173 (16)	0.0053 (14)	−0.0050 (18)
C3	0.066 (2)	0.062 (2)	0.060 (2)	0.0091 (16)	0.0209 (16)	−0.0060 (16)
C4	0.0433 (17)	0.090 (3)	0.0530 (18)	0.0062 (17)	0.0166 (14)	0.0098 (18)

Geometric parameters (Å, º)

O1—C8	1.366 (3)	C16—C20	1.474 (4)
O1—C7	1.437 (3)	C1—C2	1.375 (4)
O2—C20	1.241 (3)	C1—C6	1.378 (4)
O3—C20	1.270 (3)	C1—C7	1.501 (4)
O3—H3A	1.20 (5)	C6—C5	1.370 (4)
C8—C9	1.382 (3)	C6—H6	0.9300
C8—C13	1.394 (3)	C19—C18	1.375 (4)
C12—C13	1.369 (3)	C19—H19	0.9300
C12—C11	1.395 (3)	C7—H7A	0.9700
C12—H12	0.9300	C7—H7B	0.9700
C13—H13	0.9300	C17—C18	1.367 (4)
C14—C15	1.383 (4)	C17—H17	0.9300
C14—C19	1.400 (3)	C2—C3	1.386 (4)
C14—C11	1.485 (3)	C2—H2	0.9300
C10—C9	1.385 (3)	C18—H18	0.9300
C10—C11	1.391 (3)	C5—C4	1.368 (5)
C10—H10	0.9300	C5—H5	0.9300
C9—H9	0.9300	C3—C4	1.368 (4)
C15—C16	1.378 (3)	C3—H3	0.9300

C15—H15	0.9300	C4—H4	0.9300
C16—C17	1.391 (4)		

C8—O1—C7	117.75 (19)	C18—C19—C14	121.2 (3)
C20—O3—H3A	115 (2)	C18—C19—H19	119.4
O1—C8—C9	125.3 (2)	C14—C19—H19	119.4
O1—C8—C13	115.7 (2)	O1—C7—C1	107.2 (2)
C9—C8—C13	119.0 (2)	O1—C7—H7A	110.3
C13—C12—C11	121.8 (2)	C1—C7—H7A	110.3
C13—C12—H12	119.1	O1—C7—H7B	110.3
C11—C12—H12	119.1	C1—C7—H7B	110.3
C12—C13—C8	120.6 (2)	H7A—C7—H7B	108.5
C12—C13—H13	119.7	C18—C17—C16	119.2 (2)
C8—C13—H13	119.7	C18—C17—H17	120.4
C15—C14—C19	116.7 (2)	C16—C17—H17	120.4
C15—C14—C11	121.8 (2)	O2—C20—O3	122.5 (3)
C19—C14—C11	121.6 (2)	O2—C20—O3	122.5 (3)
C9—C10—C11	122.5 (2)	O2—C20—O3	122.5 (3)
C9—C10—H10	118.7	O2—C20—O3	122.5 (3)
C11—C10—H10	118.7	O2—C20—C16	120.1 (2)
C10—C11—C12	116.6 (2)	O2—C20—C16	120.1 (2)
C10—C11—C14	121.4 (2)	O3—C20—C16	117.4 (3)
C12—C11—C14	122.0 (2)	O3—C20—C16	117.4 (3)
C8—C9—C10	119.5 (2)	C1—C2—C3	120.6 (3)
C8—C9—H9	120.2	C1—C2—H2	119.7
C10—C9—H9	120.2	C3—C2—H2	119.7
C16—C15—C14	122.6 (2)	C17—C18—C19	121.0 (3)
C16—C15—H15	118.7	C17—C18—H18	119.5
C14—C15—H15	118.7	C19—C18—H18	119.5
C15—C16—C17	119.3 (3)	C4—C5—C6	120.3 (3)
C15—C16—C20	120.1 (2)	C4—C5—H5	119.9
C17—C16—C20	120.6 (2)	C6—C5—H5	119.9
C2—C1—C6	118.4 (3)	C4—C3—C2	120.0 (3)
C2—C1—C7	120.8 (3)	C4—C3—H3	120.0
C6—C1—C7	120.8 (3)	C2—C3—H3	120.0
C5—C6—C1	121.1 (3)	C3—C4—C5	119.6 (3)
C5—C6—H6	119.5	C3—C4—H4	120.2
C1—C6—H6	119.5	C5—C4—H4	120.2

C7—O1—C8—C9	−0.5 (4)	C8—O1—C7—C1	−175.9 (2)
C7—O1—C8—C13	179.0 (2)	C2—C1—C7—O1	90.9 (3)
C11—C12—C13—C8	−0.7 (4)	C6—C1—C7—O1	−89.1 (3)
O1—C8—C13—C12	−178.5 (2)	C15—C16—C17—C18	−0.4 (5)
C9—C8—C13—C12	1.0 (4)	C20—C16—C17—C18	178.4 (3)
C9—C10—C11—C12	0.4 (4)	C15—C16—C20—O2	2.1 (5)
C9—C10—C11—C14	179.5 (2)	C17—C16—C20—O2	−176.8 (3)
C13—C12—C11—C14	−179.1 (2)	C15—C16—C20—O2	2.1 (5)
C15—C14—C11—C10	26.6 (4)	C17—C16—C20—O2	−176.8 (3)

C19—C14—C11—C10	−153.3 (3)	C15—C16—C20—O3	−179.2 (3)
C15—C14—C11—C12	−154.4 (3)	C17—C16—C20—O3	1.9 (5)
C19—C14—C11—C12	25.7 (4)	C15—C16—C20—O3	−179.2 (3)
O1—C8—C9—C10	178.8 (2)	C17—C16—C20—O3	1.9 (5)
C13—C8—C9—C10	−0.6 (4)	C6—C1—C2—C3	1.0 (4)
C11—C10—C9—C8	−0.1 (4)	C7—C1—C2—C3	−179.1 (3)
C19—C14—C15—C16	−0.1 (4)	C16—C17—C18—C19	0.3 (5)
C11—C14—C15—C16	180.0 (2)	C14—C19—C18—C17	−0.1 (5)
C14—C15—C16—C17	0.4 (4)	C1—C6—C5—C4	0.3 (5)
C14—C15—C16—C20	−178.5 (3)	C1—C2—C3—C4	−0.9 (5)
C2—C1—C6—C5	−0.7 (4)	C2—C3—C4—C5	0.4 (5)
C7—C1—C6—C5	179.3 (3)	C6—C5—C4—C3	−0.1 (5)
C11—C14—C19—C18	179.9 (3)		

Hydrogen-bond geometry (Å, º)

*Cg*1 and *Cg*2 are the centroids of the C1–C6 and C8–C12 rings, respectively,

D—H···*A*	*D*—H	H···*A*	*D*···*A*	*D*—H···*A*
C15—H15···O2	0.93	2.48	2.791 (3)	100
C17—H17···O3	0.93	2.48	2.767 (4)	98
O3—H3*A*···O2^{i}	1.20 (5)	1.42 (5)	2.617 (3)	175 (4)
C3—H3···*Cg*1^{ii}	0.93	2.88	3.711 (4)	149
C6—H6···*Cg*1^{iii}	0.93	2.77	3.588 (4)	147
C9—H9···*Cg*2^{iv}	0.93	2.86	3.667 (3)	146
C12—H12···*Cg*2^{v}	0.93	2.81	3.629 (3)	147

Symmetry codes: (i) −*x*+1, *y*, −*z*+1/2; (ii) *x*, −*y*, *z*−1/2; (iii) *x*, −*y*+1, *z*−3/2; (iv) *x*, −*y*+1, *z*−1/2; (v) *x*, −*y*, *z*−3/2.